PHYSICAL REVIEW B

CONDENSED MATTER

THIRD SERIES, VOLUME 35, NUMBER 5 15 FEBRUARY 1987-I

Synchrotron-radiation-induced photoelectron study of some dilute $Ag_{1-x}Mn_x$ alloys

R. L. Benbow and Z. Hurych
Department of Physics, Northern Illinois University, DeKalb, Illinois 60115
(Received 19 May 1986)

Ultraviolet photoemission has been used to investigate the Mn local moment in $Ag_{1-x}Mn_x$ alloys for $x=0.02$, 0.05, 0.10, and 0.15. Both angle-resolved and angle-integrated spectra were obtained. A picture of the local moment as a scattering center emerges which is consistent with known transport properties of these alloys. On the other hand, the screening cloud around the Mn ion is sufficiently localized to exist in an $S=\frac{5}{2}$ spin state. The state is delocalized to the point that no super-Coster-Kronig transition can neutralize a $3p$ core hole, although an autoionization resonance is observed at the $3p$ core threshold. This is in contrast to metallic Mn and Mn in certain other compounds.

INTRODUCTION

The study of alloys is a technologically and scientifically important aspect of research. Alloys are created for various properties, among which are strength, hardness, weight, anticorrosion, and many other properties, usually in combination. Alloys are also found which are important in catalysis and chemical reactions. Alloys also exist as a means of isolating or creating many physical phenomena which either do not exist in elemental materials or compounds, or which are suppressed by other stronger properties of materials. For example, the Kondo effect is a phenomenon which occurs only when a small percentage of a magnetic impurity is present in a nonmagnetic host. $Ag_{1-x}Mn_x$ ($x \ll 1$) is an example of a Kondo alloy.[1,2] It is well known that addition of even minute amounts of a second metal to a good conductor will lower the conductivity. It is also an elementary fact that resistivity (the inverse of conductivity) decreases as the temperature is lowered. The Kondo effect is in contradiction to the decrease with lower T: There is a minimum in the resistivity as T is lowered toward 0 K. In addition, the resistivity in dilute *Ag*Mn alloys shows a subsequent maximum followed by a linear decrease in resistivity as T is lowered to ~ 0.1 K. *Ag*Mn alloys with dilute amounts of Mn are also known to be spin-glasses[3]—systems which show a sharp cusp in the low-field ac susceptibility at the "freezing temperature" T_f, but no Bragg reflections indicating long-range order.

The low-T behavior of *Ag*Mn with dilute amounts of Mn, as well as other alloys having nonmagnetic host materials with impurity states having stable magnetic moments, is known to be due to the exchange-split moment. Mn in noble-metal hosts exists in an almost pure $S=\frac{5}{2}$ spin state, which is referred to as a local moment.[4,5] The aim of much previous experimentation in obtaining photoemission[5–8] and optical spectra[9] has been to determine the magnitude of the energy splitting of such spin states. From photoemission,[5–8] it was found that the majority states of Mn were more than 3 eV below the Fermi energy, E_F, in *Ag*Mn, with no sign of any minority states, indicating the minority states lay almost entirely above E_F. Optical data[9] were inconclusive, showing additional structure due to the Mn, but not necessarily showing the separation between the filled and empty parts of the exchange-split spin state. Recently inverse photoemission—or bremsstrahlung isochromat spectroscopy—experiments[10–12] located the minority state some 2.1 eV above E_F in *Ag*Mn alloys.

$3d$ transition metals have recently been shown to exhibit interesting resonance phenomena as the optical excitation energy is increased through the $3p$ threshold energy. The "6-eV satellite" in Ni (Refs. 13 and 14) is an example of the resonance in which a super-Coster-Kronig (SCK) decay of a $3p$ core hole causes a two-hole final state which can also be created by direct excitation of a $3d$ electron. There is a phase relationship between these two processes which causes the resonance. To some extent, the density of empty $3d$ states affects the resonance, but the resonant satellite can be created even if there are virtually no empty $3d$ states, as in elemental Cu metal.[15,16]

In photoemission from α-manganese,[17] a giant SCK satellite appears to resonate with a valence-band satellite at the $3p$ threshold. The valence-band satellite is visible below the $3p$ threshold but not above it, so it is not clear that it is really a satellite. Photoemission studies on gas-phase Mn (Ref. 18) and on Mn in $Cd_{1-x}Mn_xSe$ (Ref. 19) show clearly that Mn goes through a resonance at the $3p$ threshold.

The present work consists of examining photoemission

data for several *Ag*Mn alloys in the spectral region including the Mn $3p$ core threshold. The aim is to see if the Mn resonance is modified by changing the environment and if further information can be obtained about the minority spin state in Mn in the alloys.

The next section gives the details of the experiment, including sample preparation and data acquisition. Following is a section detailing the results and then a discussion of the results.

EXPERIMENTAL DETAILS

Single-crystal samples of Ag, $Ag_{0.98}Mn_{0.02}$, $Ag_{0.95}Mn_{0.05}$, $Ag_{0.90}Mn_{0.10}$, and $Ag_{0.85}Mn_{0.15}$ were cut so that a (001) face was presented. The size was such that the crystals could be mounted on a molybdenum heater compatible with a standard Varian flip assembly. Prior to mounting, the crystals were mechanically polished and then etched in a solution of 50% NH_3 and 50% H_2O_2, a standard etch for Ag. The etch seemed to work in a similar manner on the *Ag*Mn alloys. In the vacuum system in which the experiment was conducted, the crystals were Ar-ion etched at low beam energies ($\sim$200—300 eV) and annealed briefly at modest temperatures (300—500 °C). Higher temperatures were found to leave the surface region of the alloys depleted of Mn. Unfortunately, neither Auger electron spectroscopy nor low-energy electron diffraction were available to monitor surface composition or structure; however, techniques were developed to check both aspects of the experimentation.

The photoemission data were obtained in two different sets of experiments. The first phase was done at relatively low photon energies (10—25 eV). The source was a MacPhereson 225 1-m normal-incidence monochromator (NIM) located on Tantalus I, the 240-MeV electron storage ring of the University of Wisconsin-Madison Synchrotron Radiation Center (SRC). Angle-resolved ultraviolet photoemission spectra (ARUPS) were obtained with a combination 127° and plane mirror analyzer (PMA for short).[20] The PMA is constructed with the plane mirror parallel to the axis of rotation of the instrument. The 127° cylindrical analyzer is the entrance state and the front end is arranged to only accept electrons with trajectories perpendicular to the axis and emitted from a point on the axis. The nature of the spectra and the symmetry displayed were consistent with the (001) face of a single crystal. A double-pass cylindrical mirror analyzer (CMA) was used to obtain angle-integrated spectra which, for the alloys, yielded spectra comparable to previously published results.

The second phase of the experimentation was carried out at the SRC on a toroidal grating monochromator (TGM) in the same vacuum system used with the NIM. The useful range of the TGM is from $\sim$20 eV to $\sim$110 eV or slightly higher. Only the CMA was used to obtain data on the TGM. Most of the data were obtained in the traditional mode of recording photoelectron energy distributions (PED's). The "extra" emissions from the Mn are always visible in the valence region of the spectra, but the Mn $3p$ core level is only apparent in spectra at photon energies greater than 50 eV above the excitation threshold. The location of the Mn $3p$ emissions provided solid evidence that Mn was present near the surface of the sample. The variation of Mn emissions from sample to sample was consistent with the nominal amount of Mn in the sample.

The data of greatest interest consist of intensity variations of the Mn valence emissions (the local moment) as the photon energy $h\nu$ was increased from several eV below the Mn $3p$ core threshold to 20—25 eV above the same threshold. PED's were obtained at 1.0- or 0.5-eV $h\nu$ intervals. As the conduction band of Ag is essentially structureless—i.e., a plateau—in this region, the intensity of the Mn emissions superimposed on the plateau are easily obtained. Best results were obtained by subtracting a Ag PED taken at the same energy as the alloy PED. The resulting difference spectra were normalized to the photon flux of the monochromator and the beam in the storage ring. Numerical integrals of the regions from -3.8 to -2.0 eV initial energy of these different spectra were obtained. The resulting integrals were plotted point-by-point *versus* photon energy. This amounts an indirect means of obtaining a constant initial-energy spectrum (CIS) as would be obtained by synchronously scanning the CMA retarding voltage along with the photon energy such that $h\nu - E_{\mathrm{CMA}} = E_i = \text{const}$.

Constant final-energy spectra (CFS's) can be obtained by holding the CMA energy constant at a low kinetic energy (typically 4—15 eV) and scanning the photon energy. Traditionally, the CFS method is sensitive to Auger transitions near core excitation thresholds if those transitions result in increased photoyield rather than obvious structure in the PED's. The CFS's usually bear a resemblance to the light-flux curve of the monochromator, so that dependence has to be removed, usually by dividing the CFS by the yield curve for the monochromator. An alternative method was used here: Since this is a study of dilute *Ag*Mn alloys, most of the structure in the CFS's was still due to the Ag host. CFS's were obtained for a Ag crystal and a "composite" CFS for Ag was obtained which represented the partial photoyield of Ag *and* flux of the monochromator. The alloy CFS's were then normalized to the Ag CFS in order to remove both the Ag and the monochromator yield dependences.

RESULTS

A. Low-energy angle-resolved results

The $Ag_{0.95}Mn_{0.05}$ and $Ag_{0.9}Mn_{0.1}$ samples were both examined in the light of angle-resolved photoelectron spectroscopy (ARPES) with the PMA. The PMA was mounted so as to accept electrons emitted into the plane of incidence of the light on both the incident and reflected sides of the sample normal, as shown in the inset in the upper portion of Fig. 1. The PMA could be rotated continuously from one position to the other. The angle of incidence of the light was 70°. The large angle of incidence has a striking effect on the emissions from the Ag host. In Figs. 1 and 2 the two PED's sample symmetric regions of $\mathbf{k}$ space but the Ag d-band emissions (between initial energies of -8.0 to -4.0 eV) have different shapes for the "+" and "−" angles. Equally striking is the

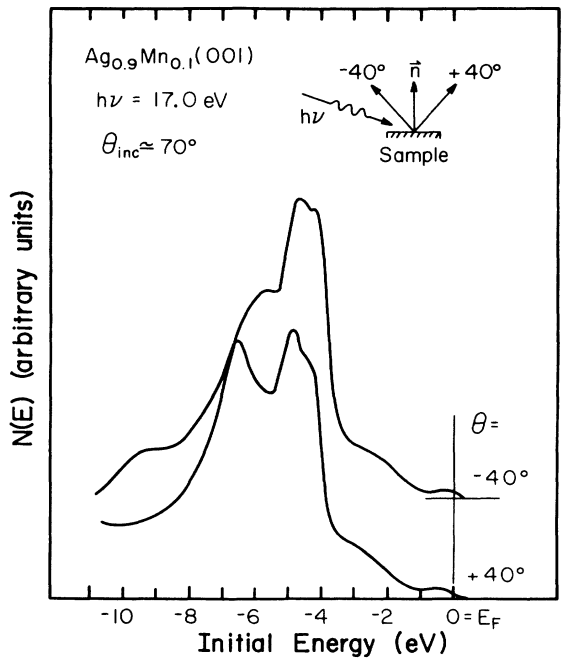

FIG. 1. ARPED's for $Ag_{0.90}Mn_{0.10}$(001) at $h\nu=17.0$ eV. The emissions are collected at $\theta=\pm 40°$ in the plane of incidence. The emissions from the d band are different in appearance because of the asymmetry of the angle of incidence relative to the two angles of emission. The VBS (~ -4.0 to -2.0 eV) is largely unaffected.

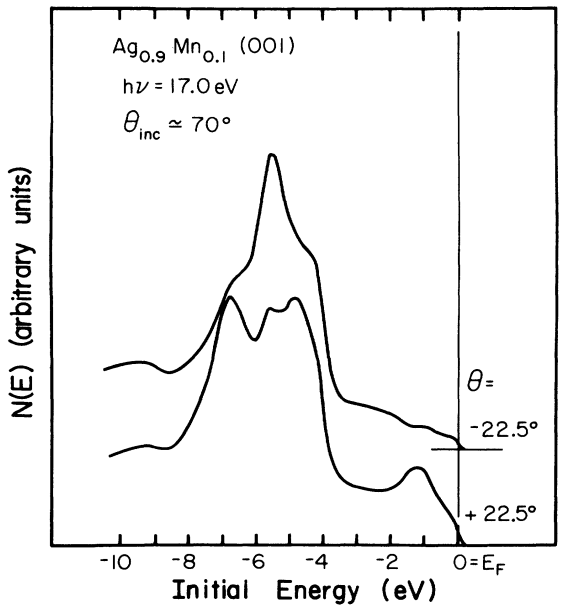

FIG. 2. Similar to Fig. 1, but $\theta=\pm 22.5°$. The VBS is still between ~ -4.0 and -2.0 eV, but is partially obscured by the presence of the Ag conduction band at ~ 1.2 eV. Again, the asymmetry of the angle of incidence relative to the two directions of emission is responsible for the differences in the Ag emissions.

conduction-band emission, found at ~ -1.2 eV in the $+22.5°$ PED in Fig. 2. The same feature is found at $-22.5°$, but is greatly suppressed. The differences in the Ag emissions arise from the different values of $\mathbf{A}\cdot\mathbf{p}$ on the different sides of the sample normal. $\mathbf{A}$ is the vector potential of the incident photon field, and $\mathbf{p}$ is the dipole (momentum) matrix element for transitions from the initial state to the final state which appear in the PED's. The contributions to the PED's from Mn are mostly unaffected by this same difference in emission angles. Neither the intensity nor the position in the PED of the Mn emissions were seen to change appreciably with angle at any $h\nu$. In Fig. 3, we present normal emission PED's from both Ag(001) and a similar crystal of $Ag_{0.9}Mn_{0.1}$ at $h\nu=17.0$ eV. The d bands are similar and the Ag conduction band is evident on both. When the Ag PED is subtracted from the alloy PED, the residual between -4.0 and -1.0 eV is interpreted as the Mn contribution. The shape of those emissions is clearly affected by the Ag conduction band—probably due to a slight misalignment of the analyzer relative to one sample when compared to the other. The relative intensity of the PED's at energies less than the d-band emission energy is due to two probable causes. First, the analyzer was in a developmental stage when these data were accumulated and subtle modifica-

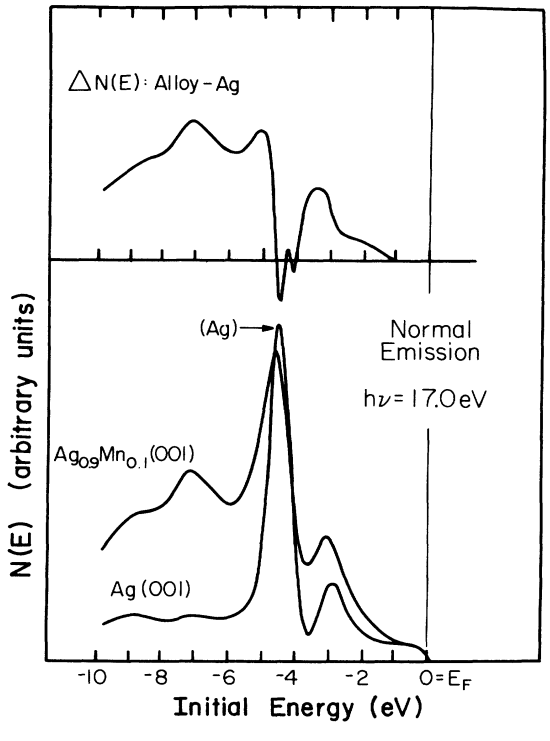

FIG. 3. Normal emission ARPED's at $h\nu=17.0$ eV for Ag(001) and $Ag_{0.90}Mn_{0.10}$(001). The angle of incidence of the light was again 70°. The peak near -3.0 eV is mostly due to the Ag conduction band. The peak between -4.0 and -1.0 eV in the difference spectrum is attributed to the Mn VBS. The shape is affected by the Ag emissions. Note that the d band is shifted lower in energy in the alloy.

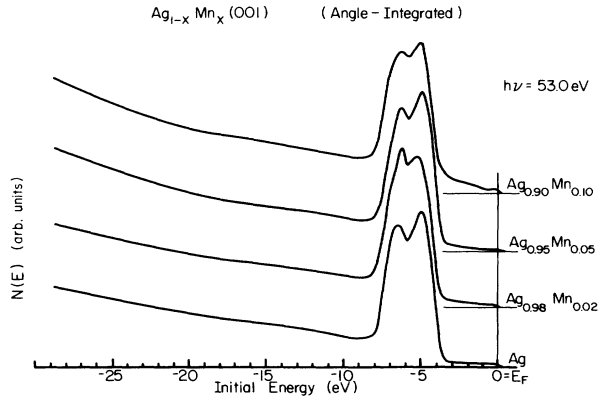

FIG. 4. Angle-integrated PED's at $h\nu = 53.0$ eV for Ag and three *Ag*Mn alloys. The photon energy is such that the VBS emissions (~ -4.0 to -2.0 eV) in the alloys are near the maximum intensity exhibited in Figs. 5–7.

tions were being continually tried to improve the low-kinetic-energy transmission of the analyzer. Second, the alloy samples produced more scattered electrons than the pure Ag sample, a clear indication of the decreased scattering length in the alloys. Other spectra at energies not showing the Ag conduction band are not so irregular in shape. A large amount of data was obtained for the alloy of Figs. 1–3 and of $Ag_{0.95}Mn_{0.05}$ and the data support two observations: (1) The Mn state is dispersionless, and (2) the Mn emissions show little intensity variation with polar- or azimuthal-angle variation.

B. High-energy angle-integrated results

The bulk of the data consists of a large set of PED's such as those shown in Fig. 4. Except for variations in the Ag d bands due to a different (100) surface orientation from sample to sample, the spectra are similar. The differences are mostly found in the region between -4 eV and E_F, where the Mn emissions appear. It is noticed, as expected, that the Mn contribution generally increases with the increased amount of Mn present in the sample. It is from PED's such as those in Fig. 4 that the CIS's in Figs. 5–7 were constructed. The Ag PED was subtracted from each of the others in turn and a numerical integral taken over the region between -3.8 and -2.0 eV. That integral then becomes a point on the CIS, which is really a difference curve. Although the overall shapes of the three curves are different, there are significant common features as well: (1) The curves are generally decreasing in intensity from low energy to high energy up to ~ 65.0 eV; (2) there is a local minimum almost exactly at the Mn $3p$ core excitation threshold (48.1 eV); (3) there is a local maximum at 51.0–51.5 eV—some 3.0–3.5 eV above the Mn $3p$ threshold.

In Fig. 8 we present selected CFS's for the alloys; all are normalized to a composite partial photoyield of Ag over the same region of photon energy. The method of normalization is apparently validated by the flatness of the normalized CFS's. Note that instead of a CFS for

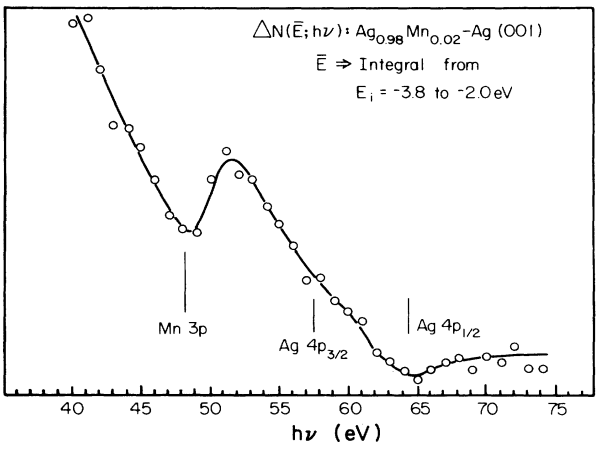

FIG. 5. CIS of VBS for $Ag_{0.98}Mn_{0.02}$. The CIS was constructed point by point from PED's of Ag and the alloy. Each point is created by taking a numerical integral of the region between $E_i = -3.8$ eV and $E_i = -2.0$ eV in the alloy and subtracting the similar integral in Ag. Both spectra were normalized to the light flux from the monochromator and the beam currents before the subtraction.

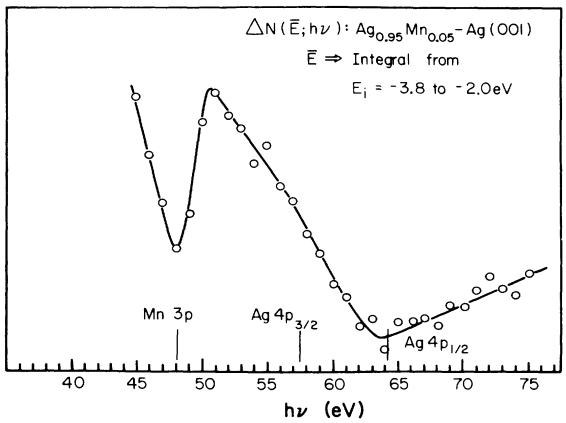

FIG. 6. Same as Fig. 5 but for $Ag_{0.95}Mn_{0.05}$.

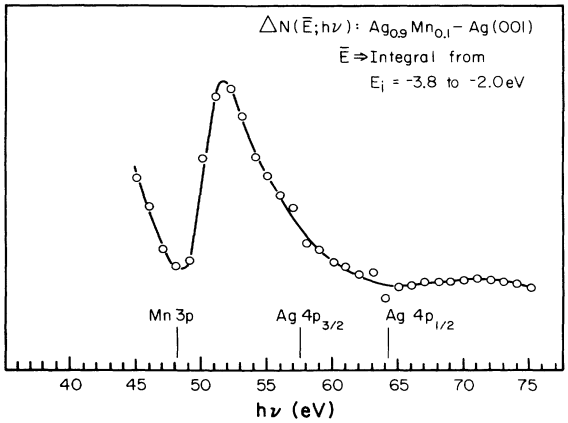

FIG. 7. Same as Fig. 5 but for $Ag_{0.90}Mn_{0.10}$.

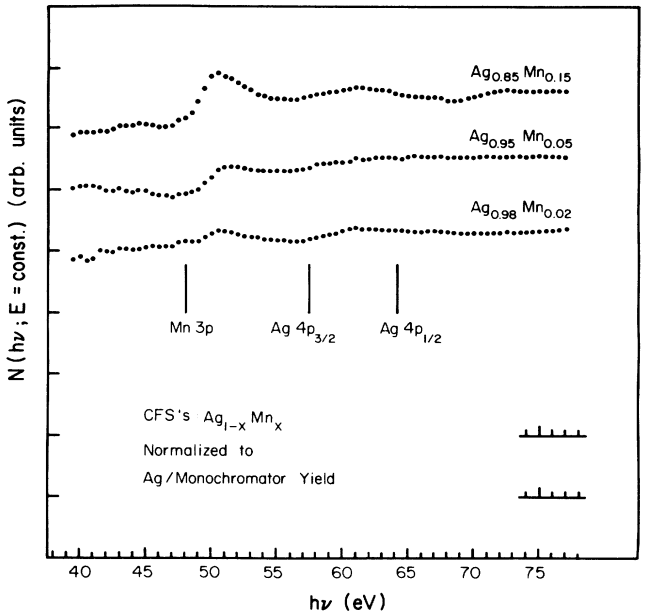

FIG. 8. CFS's for three *Ag*Mn alloys. The kinetic energy for $Ag_{0.98}Mn_{0.02}$ was 7.0 eV; for $Ag_{0.95}MN_{0.05}$, 7.0 eV; and for $Ag_{0.85}Mn_{0.15}$, 10.0 eV. All three were normalized to a composite Ag CFS, corrected for beam current decay, and made in a continuous scan.

$Ag_{0.9}Mn_{0.1}$ we present one for $Ag_{0.85}Mn_{0.15}$. Through an oversight, no suitable CFS for $Ag_{0.9}Mn_{0.1}$ was obtained. On the other hand, it is evident from our data that the $Ag_{0.85}Mn_{0.15}$ sample was annealed at too high a temperature and that the surface, or photoemission, region was partially depleted of Mn. However, the CFS is a partial photoyield at low kinetic energy. Thus the CFS measures a yield of scattered electrons which can arise from deeper within the crystal, and even for a surface region (4—6 Å) partially depleted of Mn, the CFS is expected to reflect the bulk concentration of Mn.

The salient feature common to all three CFS's is the peak at about 50.5 eV, the intensity of which is approximately proportional to the concentration of Mn. This peak in each case occurs about 2.5 eV above the Mn $3p$ photoexcitation threshold. Note that this is about 0.5—1.0 eV lower than the similar peak in the CIS's—a significant difference. Further, there is not necessarily a minimum preceding the peak—it seems to rise above the background.

DISCUSSION

A. Angle-resolved results

The traditional picture of a virtual bound state (VBS) (Refs. 21 and 22) starts with a large positive charge imbedded in an otherwise uniform matrix of a metal of lower valency. This is the case of Mn in Ag. The Mn ion will have $\sim +5$ more charge than the Ag ions. The Mn $3d$ electrons have a binding energy such that they overlap the Ag conduction band, are degenerate with it, and interact with it, thus becoming itinerant. However, the charge neutrality of the crystal demands that a screening charge—the VBS—be set up around the Mn ion. In the case of transport properties of such an impurity state, the VBS introduces increased scattering. For a Kondo system, the additional requirement of having the VBS possess a spin magnetic moment is imposed.

In the angle-resolved photoelectron energy distributions (ARPED's) the concept of a scattering center is not inconsistent with the data, which show the VBS emissions as dispersionless and with little intensity variation upon a change of angle. However, the high-energy data are more consistent with a bound state. The independence of the Mn intensity on angle and the complete absence of dispersion of the state with angle shows that the local impurity potential is far more important than the crystal potential which would tend to at least affect the intensity as the direction of emission is varied.

B. High-energy results

Sugawara *et al.*[17] have investigated the resonant properties of α-Mn over the range 30 eV $\leq h\nu \leq 130$ eV, and have observed resonant behavior in the emissions from the top of the d band near E_F. The other d-band structures show enhanced emission above the $3p$ threshold, but do not appear to be resonant in the same sense: The top of the d band has a minimum in intensity at the $3p$ threshold, while the others do not. The SCK emission is very strong and, at threshold seems to overlap a feature which may be a satellite. This feature is not in evidence at photon energies well above the onset of the SCK emissions.

In Figs. 5—7 we show the behavior of the Mn VBS emission intensity as a function of $h\nu$ for three alloys. All three were found to show the same behavior—a minimum almost exactly at the Mn $3p$ threshold energy, followed by a maximum some 3.0—3.5 eV higher in energy. This maximum seems to be about 1.0 eV lower in energy than the similar d-band feature in α-Mn relative to the $3p$ threshold and in the optical absorption coefficient of Mn.[24]

In conjunction with the CIS's of Figs. 5—7, we examine the CFS's of Fig. 8, again for three alloys, normalized so as to minimize the Ag contribution to each CFS. Again, we emphasize the region near the Mn $3p$ threshold. There is no systematic behavior below the threshold; there may or may not be an associated dip at the threshold. Additional spectra not shown here are inconsistent in that some show a dip, and others do not. All spectra do show a peak, approximately related to the amount of Mn, which is at maximum intensity some 2.5—3.0 eV above the threshold, about 0.5—1.0 eV lower in energy than the peaks in the CIS's. We interpret these curves to represent better the optical absorption than the CIS's, as they show less tendency toward complications due to any resonance. If the peak near $h\nu = 51$ eV is representative of $3p \rightarrow 3d$ transitions in Mn, then the empty part of the VBS, or local moment, should be 2.5—3.0 eV above E_F, somewhat higher than observed in the inverse photoemission experiment. A possible explanation of the difference may lie in the fact that the inverse photoemission does not create a core hole. The configuration interaction involving the op-

tically excited $3p$ core hole raises the energy of the empty d states, thus causing a slight shift in the apparent density of empty states. This is similar to the delayed onsets in autoionization for the low-Z members of the $3d$ row observed by Zajac *et al.*[23] The optical absorption spectrum of metallic Mn peaks some 4.7 eV above the $3p$ threshold,[24] as does that of $Cd_{1-x}Mn_xSe$.[19] This indicates that the local moment of Mn in the alloys is modified because of the overlap with the Ag conduction band. The spatial delocalization of the charge cloud has resulted in a lowering of the energy of the empty Mn $3d$ states in the alloys.

In the matter of the peaks in the CIS's, the process appears to be a modified resonant process. It is not a true SCK-induced resonance as is the case of Ni and Cu. No feature has been found in a PED for any of these alloys which could be attributed to a Mn SCK satellite. This is said advisedly, as it is possible that an otherwise detectable satellite could be obscured under the Ag $4d$ peaks. Suffice it to be said that no feature has been observed to "step" away from the Ag $4d$ band emissions as $h\nu$ was increased well above threshold.

The present mode of resonance starts with excitation of a Mn $3p$ core hole followed by direct recombination of the electron with energy transfer to the screening cloud of electrons surrounding the Mn ion—an autoionization process. While the VBS may be organized into a local moment ($S=\frac{5}{2}$ spin state), evidently the lifetime of the local moment is too short to allow formation of an excited Coulomb-repulsion state which is necessary in a true SCK process. We have

$$3p^6 3d^5 + h\nu \rightarrow 3p^5 3d^6 \rightarrow 3p^6 3d^4 + e^- , \quad (1)$$

which resonates with the direct process,

$$3p^6 3d^5 + h\nu \rightarrow 3p^6 3d^4 + e^- . \quad (2)$$

The final state is the same in (1) and (2). This is contrasted with the SCK mechanism

$$3p^6 3d^5 + h\nu \rightarrow 3p^5 3d^6 \rightarrow (3p^6 3d^4)^* + e^- , \quad (3)$$

where the $(3p^6 3d^4)^*$ is an excited state causing the electron in (3) to be emitted with lower energy. The direct recombination mechanism is in evidence in Ni for the emissions from the top of the (d) conduction band. It has nothing to do with the satellite resonance in Ni metal. This mechanism is also in evidence in the α-Mn data for the part of the d-band near E_F. Absent in our VBS, then, is the SCK decay mechanism present in α-Mn. The absence of the SCK satellites is further evidence that the local moment in the alloys is strongly modified from those in α-Mn or in $Cd_{1-x}Mn_xSe$.[19] The spatial delocalization has been sufficient to broaden the energy of the occupied states, lower the energy of the empty states and remove correlation with the $3p$ core hole. The energy broadening is accompanied by a reduction in lifetime of the excited Mn $5d$ states to the point that a SCK process cannot occur.

It is relevant to report that the CFS's were normalized to the Ag CFS, not only to suppress the Ag emissions, but also to enhance the contribution of the Mn effects. If the method is sound, the result would be of the form

$$I(h\nu) = I_0[1 + \delta_{Mn}(h\nu)] , \quad (4)$$

where I_0 is an arbitrary scale factor. $\delta_{Mn}(h\nu)$ is the contribution due to the Mn. In fact, we seem to have

$$I(h\nu) = I_0[1 + \delta_{Mn}(h\nu) + \Delta(h\nu)] , \quad (5)$$

where the extra term, $\Delta(h\nu)$, is due to differences between the condition of the Ag surface and those of the alloys. In Fig. 8 each curve is plotted relative to the correct base line, and it is seen that the form (5) is valid. The overall intensity is relatively flat, but $\delta_{Mn}(h\nu)$ is evidenced by the step at the Mn $3p$ threshold. The terms $\Delta(h\nu)$ are manifested by the nonrepeatability from sample to sample of other structures in the CFS's. The overall increase in photoyield above the Mn $3p$ threshold is due to the increased optical absorption and not due to any special decay process.

CONCLUSION

In summary, then, we have examined both ARUPS and resonant photoemission in several *Ag*Mn alloys. The ARUPS data show that the VBS is primarily a scattering center. The VBS is a state broad in energy and, as such, it shows no dispersion with polar angle or photon energy. The VBS also does not display very much variation in intensity as the polar angle is changed.

The VBS does change intensity in angle-integrated PED's as $h\nu$ is increased through the Mn $3p$ photoexcitation threshold. The Mn $3p$ core state is responsible for an autoionization resonance, but there is no evidence for a SCK resonance. Although the VBS can exist with spin-correlation sufficient to produce the $S=\frac{5}{2}$ local moment, it cannot be transformed into an excited Coulomb-repulsion state, presumably because the lifetime of such a state is too short.

ACKNOWLEDGMENTS

The support of the staff of the SRC is deeply appreciated. Operation of the SRC is supported by National Science Foundation (NSF) Grant No. DMR-83-13523. This work was supported by NSF Grant No. DMR-8405-173. One of us (R.L.B.) wishes to express appreciation to Professor D. W. Lynch of Iowa State University and the Ames Laboratory for the cooperation extended in procuring the alloy samples used in this experiment.

[1] D. Jha and M. H. Jerico, Phys. Rev. B **3**, 147 (1971).

[2] D. A. Tindall, M. H. Jerico, and D. Jha, Phys. Rev. B **9**, 3113 (1974).

[3] K. H. Fischer, Phys. Status Solidi B **116**, 357 (1983) (a review article).

[4] M. D. Daybell and W. A. Steyert, Rev. Mod. Phys. **40**, 380 (1968).

[5] H. S. Reehal and P. T. Andrews, J. Phys. F **10**, 1631 (1980).

[6]Lars Walldén, Philos. Mag. **21**, 571 (1970).
[7]C. Norris and L. Walldén, Solid State Commun. **7**, 99 (1969).
[8]H. Höchst, P. Steiner, and S. Hüfner, Z. Phys. B **38**, 201 (1980).
[9]H. P. Myers, L. Walldén, and Å. Karlsson, Philos. Mag. **18**, 725 (1968).
[10]D. van der Marel, G. A. Sawatsky, and F. U. Hillebrecht, Phys. Rev. Lett. **53**, 206 (1984).
[11]D. van der Marel, C. Westra, G. A. Sawatsky, and F. U. Hillebrecht, Phys. Rev. B **31**, 1936 (1985).
[12]R. G. Jordan, W. Drube, D. Straub, and F. J. Himpsel, Phys. Rev. B **33**, 5280 (1986).
[13]C. Guillot, Y. Ballu, J. Paigne, J. Lecante, K. P. Jain, P. Thiry, R. Pinchaux, Y. Petroff, and L. M. Falicov, Phys. Rev. Lett. **39**, 1632 (1977).
[14]M. R. Thuler, R. L. Benbow, and Z. Hurych, Phys. Rev. B **27**, 2082 (1983).
[15]M. Iwan, F. J. Himpsel, and D. E. Eastman, Phys. Rev. Lett. **43**, 1829 (1979).
[16]M. R. Thuler, R. L. Benbow, and Z. Hurych, Phys. Rev. B **26**, 669 (1982).
[17]H. Sugawara, A. Kakizaki, I. Nagakura, and T. Ishii, J. Phys. F **12**, 2929 (1982).
[18]M. O. Krause, T. A. Carlson, and A. Fahlman, Phys. Rev. A **30**, 1316 (1984).
[19]A. Franciosi, Shu Chang, R. Reifenberger, U. Debska, and R. Reidel, Phys. Rev. B **32**, 6682 (1985).
[20]The analyzer was designed and constructed by Dr. Neville V. Smith of AT&T Bell Laboratories. We have used it with the gracious consent of Dr. Smith.
[21]J. Friedel, Suppl. Nuovo Cimento **7**, 287 (1958).
[22]P. W. Anderson, Phys. Rev. **124**, 41 (1961).
[23]G. Zajac, S. D. Bader, A. J. Arko, and J. Zak, Phys. Rev. B **29**, 5491 (1984).
[24]B. Sonntag, R. Haensel, and C. Kunz, Solid State Commun. **7**, 597 (1969).